New Thiazole Derivatives: Potent Antifungal against *Candida albicans*, with *silico* Docking Unveiling Key Protein Interactions

Rebaz A. Omer[1,2†], Karzan M. Ahmed[3], Khdir A. Othman[1], Wali M. Hamad[1], Rahman K. Faraj[4], Ali J. Muhialdin[5] and Shalaw K. Salih[1]

[1]Department of Chemistry, Faculty of Science and Health, Koya University, Koya, KOY45, Kurdistan Region – F.R. Iraq

[2]Department of Pharmacy, College of Pharmacy, Knowledge University, Erbil 44001, Kurdistan Region – F.R. Iraq

[3]Department of Chemistry, College of Education, University of Garmian, Kalar 46021, Kurdistan Region – F.R. Iraq

[4]Department of Chemistry, College of Science, University of Garmian, Kalar 46021, Kurdistan Region – F.R. Iraq

[5]Department of Animal Production, College of Agricultural Engineering Sciences, University of Garmian, Kifri 46022, Kurdistan Region – F.R. Iraq

***Abstract*—While bacterial superbugs have garnered much attention, the rise of antifungal resistance poses a growing threat. This study explores the potential of newly synthesized 2,5-Bis(3,4-Dialkoxy Phenyl) Thiazolo[5,4-d] Thiazoles (DATTn compounds) as antifungal agents. Notably, DATTn compounds demonstrated significant fungicidal activity against *Candida albicans*, a major fungal pathogen, whereas remaining largely ineffective against common bacterial strains, such as *Staphylococcus aureus* and *Escherichia coli*. *In silico* docking simulations using Schrödinger suites unveiled the molecular basis for this selectivity, revealing strong interactions between DATTn molecules and a crucial fungal protein (Portion Data Bank ID: 8JZN) in *C. albicans*. These findings highlight the potential of DATTn compounds as promising leads for the development of novel antifungal therapies, particularly in light of escalating drug resistance concerns.**

***Index Terms*—Antifungal activity, Bacterial resistance, Candida albicans, DATTn compounds, Drug discovery, Molecular docking.**

I. Introduction

In recent years, the scientific community's fascination with heterocyclic mesomorphic compounds has surged, driven by the remarkable mesomorphic properties exhibited by these molecules (Omer, et al., 2023b, Omer, Koparir and Koparir, 2023a). This growing interest is attributed not only to the potential for discovering novel mesogenic substances in heterocyclic chemistry but also to the profound influence of heteroatoms, including sulfur, oxygen, and nitrogen, on the formation and behavior of mesophases. These heteroatoms confer unique properties on heterocyclic compounds, making them versatile candidates for various applications (Salih, et al., 2023; Omar, et al., 2023b). This study focuses on a specific class of heterocyclic mesomorphic compounds known as 2,5-Bis(3,4-dialkoxy phenyl) Thiazolo[5,4-d] thiazoles, collectively referred to as $DATT_n$ compounds. These compounds have garnered attention not only for their inherent mesomorphic properties but also for their potential to revolutionize diverse scientific domains including materials science, liquid crystal displays, and antimicrobial research (Al-Mutabagani, et al., 2021; Atmaram and Roopan, 2022). In the context of antimicrobial research, pathogens such as *Staphylococcus aureus*, *Escherichia coli*, and *Candida albicans* present significant global challenges (Omar, Omar and Abdullah, 2016a, Omar, Smail and Omar, 2016b). *S. aureus*, responsible for a spectrum of infections from skin ailments to life-threatening diseases, necessitates targeted intervention strategies. *E. coli*, a notorious bacterium, plays a role in various infections, including urinary tract infections and foodborne illnesses. *C. albicans*, a fungal pathogen, is associated with conditions such as candidiasis, posing a particular challenge, especially for immunocompromised individuals (Omer, et al., 2019; Koparir, et al., 2022).

This research takes a multifaceted approach to evaluate the antimicrobial potential of newly synthesized compounds. *In*

ARO-The Scientific Journal of Koya University
Vol. XII, No. II (2024), Article ID: ARO.11557. 13 pages
DOI: 10.14500/aro.11557
Received: 29 February 2024; Accepted: 19 June 2024
Regular research paper: Published: 25 July 2024
†Corresponding author's e-mail: rebaz.anwar@koyauniversity.org

vitro experiments rigorously examine these compounds' ability to inhibit the growth of the mentioned pathogens *S. aureus*, *E. coli*, and *C. albicans*. Precise experimentation allows the determination of their minimum inhibitory concentrations (MIC) and minimum bactericidal concentrations (MBC), providing insights into their effectiveness against these pathogens. Furthermore, the *in silico* research involves molecular docking using the Schrödinger Suite, specifically the version released in 2023, to gain a deeper understanding how these compounds interact with specific proteins or molecular pathways intrinsic to the targeted pathogens. In the case of *S. aureus*, two critical targets, penicillin-binding protein 2a (PBP2a) and D-Ala: D-Ala ligase, have been selected for their roles in cell wall integrity. In *E. coli*, DNA gyrase, vital for DNA replication, is the target of interest. For *C. albicans*, beta-glucan synthase, a fundamental component of the fungal cell wall, is strategically addressed. Inhibition of these targets is aimed at weakening the pathogens, rendering them more susceptible to immune defenses and conventional antimicrobial agents.

II. Experimental and Methods

A. In Vitro Section

Synthesis of 2,5-Bis(3,4-dialkoxy phenyl) Thiazolo[5,4-d] thiazoles (DATTn) was completed using the technique published in previous work (Salih, et al., 2023). Subsequently, its molecular structure was verified through Fourier-transform infrared spectroscopy, ^{1}H-NMR, and ^{13}C-NMR analysis (Hamad, Aziz, and Al-Dujaili, 2004), with the 3,4 positions of the two benzene rings substituted (R = CnH_2n+1, n = 2–10) (Fig. 1). The materials used in the study as samples were (DATTn compounds), S. aureus is a multidrug-resistant Gram-positive bacterium, E. coli is a broad-spectrum beta-lactamase, and C. albicans is a fungal infection. Supporting materials are nutrient agar, nutrient broth, and dimethyl sulfoxide (DMSO) from Sigma Aldrich in Turkey.

B. Preparing Serial Dilutions

The solution of each compound was prepared by adding 0.001 g of the compound into the 1 mL of DMSO solvent, drawn 0.1 mL of each compound (DATT 2, 3, 4, 5, 6, 7, 8, 9, and 10), and added into 0.9 mL of nutrient broth (tube 1) and then 0.1 mL from tube 1 into the second tube, from it into the third tube, and so on. However, the final drawing mixture was discarded. Finally, serial dilutions of each compound in nutrient broth were prepared, as shown in Table I.

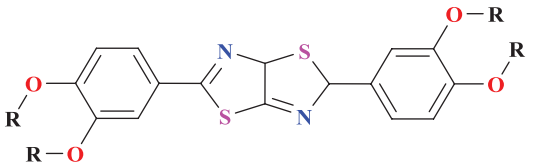

2,5-Bis(3,4-dialkoxy phenyl) Thiazolo[5,4-d] thiazoles **(DATT$_n$)**

(R= C_nH_{2n+1} n = 2-10)

Fig. 1. General molecular structure of study compounds.

C. Microbial Inoculation

A loopful of each of the bacterial strain's colony and yeast colony was inoculated in a nutrient broth tube and incubated at 37°C for 24 h. After the visibility growth of each strain, and adjusted it to 0.5 McFarland by *DensiCHEK* device (BioMerieux/French), 10 µL of each strain was added into each dilution and then incubated for 24–48 h. After incubation time, a loopful of each tube contents was subcultures utilizing striking on nutrient agar and incubated for 24–48 h. The results were read to the end of the visible growth of colonies.

III. Results and Discussion

A. In Vitro

The compound (DATTn compounds) has been synthesized and its antibacterial and fungicidal activity has been evaluated by serial dilution method (National Committee for Clinical Laboratory Standard, 2020). To determine the antimicrobial activity of the DATTn compounds, a serial concentration analysis (DATT 2, 3, 4, 5, 6, 7, 8, 9, and 10) were conducted, as shown in Table I. This analysis aims to evaluate the antibacterial and fungicidal activity of the DATTn compounds against various strains, including Gram-positive *S. aureus*, Gram-negative *E. coli*.

To obtain accurate scientific results, tubes containing the final concentrations of the DATTn compounds were inoculated with a standard microbial suspension (10 µL of 10^5 CFU/mL strains of *S. aureus*, *E. coli*, and *C. albicans*) in tubes with nutrient broth to determine the MIC and MBC values for each strain. After making all the preparations, the tubes were incubated aerobically at 35°C for 24–48 h. After an overnight incubation period at 35°C, the tubes were examined for visible bacterial growth as indicated by turbidity. Three control tubes were maintained for each strain (media control, *in vivo* control, and extraction control). The lowest concentration (highest dilution) of a compound that did not result in visible growth (no turbidity) in the first 24 h when compared to control tubes is considered the initial MIC. Dilutions that showed no turbidity were incubated for an additional 24 h at 35°C. The lowest concentration that did not result in visible turbidity after a total incubation period of 48 h was considered the MIC. All concentration was determined by sub-cultivation (which showed no visible turbidity) on fresh nutrient agar medium. The plates were incubated for 24–48 h at 35°C. It is seen from the data presented in Table II that (DATTn compounds) exhibits antifungal activity with respect to the test cultures under study. It appears that the test culture of *C. albicans* demonstrated the same susceptibility level to DATT 2, 3, 4, 5, 6, and 7 compound concentrations but moderately to DATT 8, 9, and 10. *S. aureus* with coccus shape was resistant to all compound concentrations (DATT 2, 3, 4, 5, 6, 7, 8, 9, and 10) by dilution method. Furthermore, *E. coli* was resistant to compound concentrations (DATT 2, 3, 4, 5, 6, 7, 8, 9, and 10) by the dilution method. Through the experimental procedure, we found that the concentration

TABLE I
Chemical Structure and Molecular Weight of $DATT_n$ Compounds with Delusions Used

No.	Name of compounds	Chemical structures	Molecular weight	Molarity	Serial dilutions
1	$DATT_2$	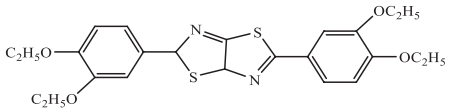	472.62	0.0021	0.0021–0.00052
2	$DATT_3$	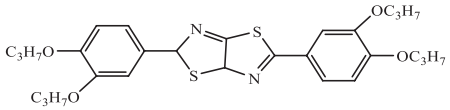	528.73	0.0019	0.0019–0.00047
3	$DATT_4$	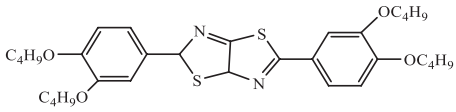	584.83	0.0017	0.0017–0.00042
4	$DATT_5$	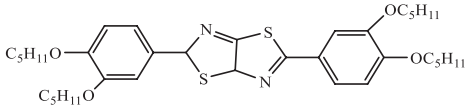	640.94	0.0015	0.0015–0.00037
5	$DATT_6$	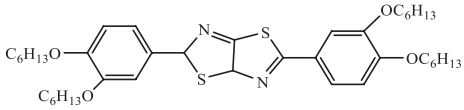	697.05	0.0014	0.0014–0.00035
6	$DATT_7$	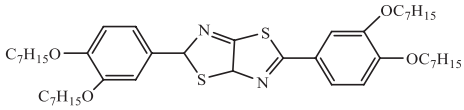	753.16	0.0013	0.0013–0.00032
7	$DATT_8$	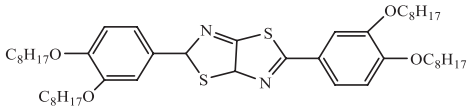	809.27	0.0012	0.0012–0.0003
8	$DATT_9$	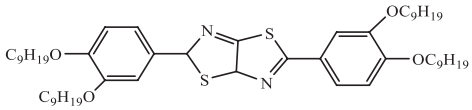	865.37	0.0011	0.0011–0.00027
9	$DATT_{10}$	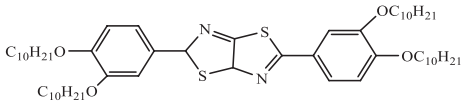	921.48	0.001	0.001–0.00025

TABLE II
Effects of Compounds on Bacterial and Fungal Growth

No.	Name of compounds	*Staphylococcus aureus*	*Escherichia coli*	*Candida albicans*
1	$DATT_2$	+	+	−
2	$DATT_3$	+	+	−
3	$DATT_4$	+	+	−
4	$DATT_5$	+	+	−
5	$DATT_6$	+	+	−
6	$DATT_7$	+	+	−
7	$DATT_8$	+	+	±
8	$DATT_9$	+	+	±
9	$DATT_{10}$	+	+	±

(+) growth of microbes *or* the compounds not effective, (−) not growth of microbes *or* the compounds kills the microbes, (±) low growth of microbes *or* the compounds effective moderately

of $DATT_7$ did not result any growth after a total incubation, which is considered the MIC. Therefore, our results revealed the importance of DATTn compounds when associated with antifungal, to control resistance, which has become a threat to human health.

B. Targeting Proteins across Pathogens

The pathogens *S. aureus*, *E. coli*, and *C. albicans* are causative agents of diverse infections in humans. The mitigation of these infections through molecular docking necessitates the precise targeting of specific proteins or molecular pathways intrinsic to these pathogens (Moravej, et al., 2018; Koparir, et al., 2023a; Khan, et al., 2023). Viable targets encompass enzymes implicated in cell wall biosynthesis, host cell adhesion, toxin production, and virulence factors. The molecular docking process encompasses target identification, 3D structure acquisition, compound screening for binding interactions, binding affinity prediction, and experimental compound validation. The study has focused on specific proteins of E. coli, and S. aureus, which have been carefully chosen for inhibition (Rementeria, et al., 2005; Ruer, et al., 2015; Anwar Omar, et al., 2023).

S. aureus

Identified two critical targets within the pathogenic bacterium S. aureus that are essential for cell wall integrity. The first target is PBP2a, labeled as 5M18 in the Portion Data Bank (PDB). PBP2a, a member of the Penicillin-Binding

Proteins (PBPs) family, is centrally involved in peptidoglycan synthesis. Inhibiting PBPs disrupts the cell wall, rendering *S. aureus* more susceptible to immune defenses and antibiotics. Protein 5M18 features a high-resolution structure (1.98 Å) (Fishovitz, et al., 2014; Verma, et al., 2022; Mahasenan, et al., 2017; Koparir, et al., 2023b). The second target was found in PDB entry 3N8D (crystal structure of *S. aureus* VRSA-9 D-Ala: D-Ala ligase), which offers the crystal structure of *S. aureus* VRSA-9 D-Ala: D-Ala ligase. This enzyme is a key contributor to cell wall synthesis. The structural data it provides are indispensable for potential antibiotic development, particularly when addressing antibiotic-resistant *S. aureus* strains. Protein 3N8D exhibits a reasonable resolution (2.3 Å) and solid refinement. Its lattice parameters and symmetry are well defined. Further analysis involves exploring the protein's three-dimensional structure and identifying potential ligand-binding sites (Lebreton and Cattoir, 2019; Paymal, et al., 2023; Omar, et al., 2023a). Together, these two targets present a multifaceted strategy for weakening *S. aureus* by compromising its cell wall integrity.

E. coli

We have chosen DNA gyrase as our docking target due to its pivotal role in DNA replication within *E. coli*. With good-resolution structure and well-defined parameters, such as those found in the DNA binding and cleavage domain (PDB ID: 6RKU), it serves as an ideal candidate for molecular docking studies. This selection enables us to precisely understand how our molecules interact with DNA gyrase, ultimately disrupting DNA replication and leading to the demise of bacterial cells (Nöllmann, et al., 2007; Jakhar, et al., 2022).

C. albicans

Beta-glucan synthase, denoted by PDB ID, has been strategically chosen with a resolution (2.47 Å) structure and well-defined parameters. This enzyme plays a pivotal role in the synthesis of beta-glucans, a fundamental constituent of the fungal cell wall. The inhibition of this enzyme significantly weakens the fungal cell wall, rendering *C. albicans* more susceptible to host immune defenses and antifungal agents (Liu and Balasubramanian, 2001; Zhao, et al., 2023).

C. Docking Studies on Proteins

Schrödinger's "LigPrep" tool in Maestro 13.5 was used to generate three-dimensional models of the synthesized compounds ($DATT_{2-10}$). These models were prepared to create the chemical structures. To ensure accurate binding interactions, the "Protein Preparation Wizard" in Schrödinger's suite was utilized for proteins 5M18, 3N8D, 6RKU, and 8JZN. This process involved adding missing hydrogen atoms, correcting ionization states, formal charges, bond orders, and applying the OPLS4 force field (Chen, et al., 2023a). For a comprehensive evaluation of protein binding sites for $DATT_n$ molecules, the SiteMap panel within Maestro was employed. Following the identification of these binding sites, the Glide Grid tool was instrumental in configuring the docking environment, defining essential site characteristics. Subsequently, molecular docking with $DATT_{2-9}$ molecules was conducted to predict their interactions within the protein's binding sites. The Glide Grid played a vital role in ensuring the accuracy of these calculations by providing critical site information for the evaluation of ligand-protein interactions and the identification of potential drug candidates (Farid, et al., 2006: Halgren, 2009). The structures of $DATT_n$ molecules, generated using "LigPrep," were systematically docked into various pockets within proteins 5M18, 3N8D, 6RKU, and 8JZN, based on their specific binding site characteristics, including sitescore, size, and Dscore. To achieve precise results, the "Glide" software with extra precision (XP) was utilized, and the Induced Fit Docking workflow within Maestro was incorporated for proteins exhibiting strong binding affinity with $DATT_n$ molecules.

D. Site Selection for Effective $DATT_n$ Molecule Interactions

In the study, the SiteMap panel within the Maestro software was leveraged to predict multiple binding pockets within the molecular models of four proteins: 5M18, 3N8D, 6RKU, and 8JZN. Each protein yielded a set of five binding sites, resulting in a total of 20 distinct binding pockets under scrutiny. The primary objective was to identify the binding pocket that offered the most favorable interactions with $DATT_n$ molecules. The ensuing data (Table III) provide an overview of the key characteristics of these binding pockets. Notably, the analysis revealed that when compounds were docked with site-4 in the 8JZN protein of *C. albicans*, it produced the most promising interaction with $DATT_n$ molecules compared to the other pockets in the remaining proteins (Table IV). This alignment with experimental results suggests the potential of these molecules to effectively inhibit the enzyme (Table II), leading to a significant weakening of the cell wall of *C. albicans*. This outcome holds the promise of halting microbial growth or even eradicating the microbes entirely, marking a significant advancement in antifungal research.

E. Glide-dock_XP_8JZN-sit-4

In the context of molecular docking simulations conducted within Schrödinger Maestro, this research scrutinizes molecular interactions by assessing docking scores and XP scores. These scores encompass various factors, including van der Waals interactions, electrostatic interactions, desolvation energies, and hydrogen bonding, all of which play a pivotal role in predicting binding affinity. Lower scores are indicative of more favorable interactions between ligands and proteins. Table V presents the docking scores and XP GlideScores for a range of $DATT_n$ molecules, shedding light on their respective binding affinities to the target protein. These scores span the spectrum from $DATT_{10}$, which registers a score of −2.279, to $DATT_6$ and $DATT_8$, both of which exhibit scores of −9.760. This variance underscores the diversity in binding strengths across the compounds. Notably, there is a remarkable concurrence between the docking and XP GlideScores for each $DATT_n$ molecule, with the exception of $DATT_{10}$, which deviates as an outlier, implying potentially weaker binding. Conversely, $DATT_2$, $DATT_3$, $DATT_4$, $DATT_5$,

TABLE III
Optimal Protein Binding Sites with Highest Interaction Scores for $DATT_n$ Molecules

Title	5M18_site_1 *Staphylococcus aureus*	3N8D-site_2 *Staphylococcus aureus*	6RKU_site_2 *Escherichia coli*	8JZN_site_4 *Candida albicans*
Site score	1.003876	1.025507	1.043826	1.145268
Size	1001	256	620	300
D score	0.996551	0.970397	1.051778	1.224372
Volume	2722.391	879.109	1590.834	779.296
Exposure	0.559419	0.615038	0.479429	0.431818
Enclosure	0.703794	0.736137	0.763531	0.775485
Contact	0.891395	0.865776	0.965688	0.992804
Phobic	0.394444	0.261777	0.506718	2.2275
Philic	1.121856	1.261613	1.062394	0.554965
Balance	0.3516	0.207494	0.476959	4.013764
Don/acc	1.028832	0.816949	1.485156	0.857137

$DATT_7$, and $DATT_9$ all manifest scores surpassing the −8.122 threshold, signifying substantial promise in terms of binding affinities (Sandor, Kiss, and Keserű, 2010; Jays, Mohan, and Saravanan, 2019). Furthermore, the research delves into the assessment of ligand efficiency concerning $DATT_n$ molecules positioned within site-4 of the 8JZN protein. Ligand efficiency serves as a metric for gauging their binding effectiveness. The values encompass a spectrum from −0.036 to −0.254, with $DATT_2$ showcasing the highest efficiency at −0.254, and $DATT_{10}$ recording the lowest efficiency at −0.036. These results cast $DATT_2$ as a compelling candidate characterized by a robust binding affinity. However, it is important to acknowledge that further studies are imperative to validate its suitability for drug development (Abad-Zapatero and Metz, 2005; Hopkins, et al., 2014). Analysis of "Glide EModel" and "Glide Energy" values reveals a close correspondence across the various molecules. $DATT_6$ emerges as the frontrunner with the highest Glide EModel value at −118.419, indicative of a robust and favorable binding profile. In contrast, $DATT_{10}$ reports the lowest value at −37.813, which signifies a relatively less favorable binding profile. The rest of the molecules exhibit values that fall within this range (Vass, Tarcsay, and Keserű, 2012; Tripathi, et al., 2012). Values pertaining to "Glide EInternal" exhibit significant variability. $DATT_8$ takes the lead with the highest value of 21.881, signifying a substantial contribution of internal energy to the binding. Conversely, $DATT_4$, $DATT_5$, and $DATT_6$ display values of 0.000, denoting that their internal energy exerts minimal influence on the binding energy (Gulcin, et al., 2022). The "glide evdw" parameter highlights $DATT_9$ as the compound with the lowest van der Waals energy value at −77.755, signifying robust non-polar interactions within the protein pocket. In contrast, $DATT_2$ reports the lowest value at −52.870, indicating relatively weaker interactions. The other molecules demonstrate varying strengths in their respective interactions (Naghiyev, et al., 2022). Analysis of "XP Electro" elucidates that $DATT_5$ boasts the most negative electrostatic energy at −0.209, underscoring robust interactions, whereas $DATT_4$ registers the highest positive energy at 0.012. The other molecules exhibit differing electrostatic energies, exerting an impact on their respective binding within the protein pocket. Among the molecules, $DATT_6$ stands out with a hydrogen bond interaction value of −0.350, whereas DATT8 and $DATT_{10}$ exhibit comparatively weaker hydrogen bond interactions. In contrast, $DATT_2$, $DATT_3$, $DATT_4$, $DATT_6$, $DATT_7$, and $DATT_9$ report no notable hydrogen bonding interactions, signifying values of 0.000 (Kaka, et al., 2024). The "XP RotPenal" parameter, employed to assess ligand rotational freedom within the protein pocket, yields analogous values ranging from 0.330 to 0.342 across all molecules. This uniformity implies consistent flexibility in ligand binding, with lower values indicating a lesser degree of rotational constraint (Beinat, 2014). In the context of "XP ExposPenal," it is observed that $DATT_{10}$ incurs the highest penalty at 1.860 for exposed polar atoms, suggesting potential constraints on binding stability. In contrast, the other molecules are associated with lower or zero penalties, which allude to fewer constraints related to exposed polar atoms in the context of ligand binding (Sarafroz, Siddiqui, and Yar, 2020). Finally, scrutiny of "glide posenum" reveals that $DATT_5$ exhibits the highest conformational flexibility, offering 30 distinct binding poses. On the other hand, $DATT_{10}$ exhibits the least flexibility, characterized by a solitary binding pose. The remaining molecules present varying numbers of binding poses, underscoring their adaptability within the protein pocket (Erdoğan, Taslimi, and Tuzun, 2021). Table VI shows docking scores and binding characteristics for $DATT_n$ molecules at protein site 8JZN-sit-4.

In the conducted study, we explored the intricate interactions between $DATT_n$ molecules and the 8JZN-sit-4 protein in *C. albicans*. To visually represent these interactions, a comprehensive fingerprint interaction (Fig. 2) was generated. This figure effectively illustrates the diverse contacts occurring between $DATT_n$ molecules and the protein's binding pocket, encompassing various interaction types, including backbone, sidechain, polar, hydrophobic, aromatic, and charged residues, providing a clear overview of the binding process. To quantitatively evaluate these interactions, computational analysis was performed and the results are summarized in Table V. This table offers a quantitative assessment of the similarity between $DATT_n$ molecules and the protein, enabling researchers to compare interaction patterns across different $DATT_n$ molecules

TABLE IV
Docking Performance Metrics for Ligand Efficiency and Scoring (glide-xp) in DATTn Molecule Interactions

5M18-*Staphylococcus aureus*									
Title	$DATT_2$	$DATT_3$	$DATT_4$	$DATT_5$	$DATT_6$	$DATT_7$	$DATT_8$	$DATT_9$	$DATT_{10}$
Glide ligand efficiency	−0.108	−0.131	−0.075	−0.077	−0.073	−0.024	−0.035	−0.015	−0.032
Docking score	−3.447	−4.720	−2.994	−3.392	−3.502	−1.237	−1.948	−0.892	−2.016
XP GScore	−3.447	−4.720	−2.994	−3.392	−3.502	−1.237	−1.948	−0.892	−2.016
Glide evdw	−38.679	−35.950	−53.513	−59.394	−51.745	−60.290	−69.386	−66.366	−69.030
Glide ecoul	−7.419	−0.949	−5.115	−5.633	−3.711	−3.503	−5.252	−6.902	−7.488
Glide energy	−46.098	−36.899	−58.628	−65.027	−55.456	−63.793	−74.638	−73.268	−76.518
Glide einternal	0.000	0.000	14.549	8.684	11.026	0.000	7.101	30.423	19.701
Glide emodel	−62.869	−65.495	−73.446	−92.087	−84.403	−101.019	−110.560	−93.079	−114.995
XP HBond	−1.427	−0.268	−0.019	0.000	0.000	0.000	0.000	0.000	−0.541
XP PhobEn	0.000	0.000	0.000	0.000	0.000	0.000	0.000	0.000	0.000
XP PhobEnHB	0.000	−1.500	0.000	0.000	0.000	0.000	0.000	0.000	0.000
XP LowMW	0.000	0.000	0.000	0.000	0.000	0.000	0.000	0.000	0.000
XP RotPenal	0.233	0.316	0.323	0.336	0.341	0.342	0.340	0.335	0.330
XP LipophilicEvdW	−1.838	−2.983	−3.085	−3.386	−5.397	−2.777	−3.191	−3.006	−3.508
XP Electro	−0.556	−0.071	−0.384	−0.422	−0.278	−0.263	−0.394	−0.518	−0.562
XP ExposPenal	0.142	0.563	0.171	0.080	0.832	0.461	1.297	1.296	1.264
glide posenum	5.000	1.000	14.000	5.000	15.000	10.000	35.000	1.000	7.000
3N8D-*Staphylococcus aureus*									
Title	$DATT_2$	$DATT_3$	$DATT_4$	$DATT_5$	$DATT_6$	$DATT_7$	$DATT_8$	$DATT_9$	$DATT_{10}$
Glide ligand efficiency	−0.120	−0.136	−0.087	−0.109	−0.071	−0.058	−0.037	−0.076	−0.006
Docking score	−3.825	−4.904	−3.499	−4.797	−3.406	−3.031	−2.078	−4.556	−0.401
XP GScore	−3.825	−4.904	−3.499	−4.797	−3.406	−3.031	−2.078	−4.556	−0.401
Glide evdw	−38.856	−34.421	−48.673	−55.916	−47.490	−56.718	−57.837	−61.914	−28.325
Glide ecoul	−8.955	−10.910	−7.660	−4.414	−5.321	−3.778	−−2.763	−2.931	−1.953
Glide energy	−47.811	−45.331	−56.334	−60.330	−52.812	−60.496	−60.600	−64.845	−30.279
Glide einternal	9.591	10.785	11.031	19.182	8.949	16.441	16.736	17.774	9.544
Glide emodel	−58.857	−58.214	−77.045	−78.723	−68.386	−76.720	−80.318	−89.321	−1.856
XP HBond	−1.333	−1.876	−1.557	−0.773	−0.421	0.000	−0.350	−0.700	0.000
XP PhobEn	0.000	0.000	0.000	0.000	0.000	0.000	0.000	0.000	0.000
XP PhobEnHB	0.000	0.000	0.000	0.000	0.000	0.000	0.000	0.000	0.000
XP LowMW	0.000	0.000	0.000	0.000	0.000	0.000	0.000	0.000	0.000
XP RotPenal	0.233	0.316	0.323	0.336	0.341	0.342	0.340	0.335	0.330
XP LipophilicEvdW	−2.054	−2.525	−2.819	−4.029	−3.762	−4.474	−3.637	−5.330	−1.466
XP electro	−0.672	−0.818	−0.575	−0.331	−0.399	−0.283	−0.207	−0.220	−0.147
XP ExposPenal	0.000	0.000	0.129	0.000	0.834	0.384	0.777	0.358	0.882
glide posenum	72.000	3.000	7.000	1.000	21.000	7.000	30.000	2.000	1.000
6RKU-*Escherichia coli*									
Title	$DATT_2$	$DATT_3$	$DATT_4$	$DATT_5$	$DATT_6$	$DATT_7$	$DATT_8$	$DATT_9$	$DATT_{10}$
Glide ligand efficiency	−0.165	−0.086	−0.067	−0.071	−0.111	−0.093	−0.077	−0.013	−0.009
Docking score	−5.290	−3.088	−2.677	−3.110	−5.336	−4.811	−4.303	−0.759	−0.584
XP GScore	−5.290	−3.088	−2.677	−3.110	−5.336	−4.811	−4.303	−0.759	−0.584
Glide evdw	−52.633	−65.206	−61.157	−61.702	−58.950	−73.248	−65.615	−64.589	−74.283
Glide ecoul	−3.907	−2.179	0.282	−4.856	−3.214	−3.992	−4.051	−4.488	−4.374
Glide energy	−56.540	−67.385	−60.875	−66.558	−62.164	−77.240	−69.666	−69.077	−78.657
Glide einternal	8.603	10.345	0.000	17.200	8.961	15.148	18.866	12.609	17.759
Glide emodel	−66.950	−82.863	−79.753	−85.753	−99.824	−113.239	−98.092	−100.341	−114.929
XP HBond	−0.320	−0.257	−0.147	−1.251	−0.829	−1.385	−0.391	−0.700	0.000
XP PhobEn	0.000	0.000	0.000	0.000	−0.650	0.000	0.000	0.000	0.000
XP PhobEnHB	0.000	0.000	0.000	0.000	0.000	0.000	0.000	0.000	0.000
XP LowMW	0.000	0.000	0.000	0.000	0.000	0.000	0.000	0.000	0.000
XP RotPenal	0.233	0.316	0.323	0.336	0.341	0.342	0.340	0.335	0.330
XP LipophilicEvdW	−6.108	−6.984	−6.874	−5.993	−7.957	−7.469	−5.242	−5.129	−5.272
XP Electro	−0.293	−0.163	0.021	−0.364	−0.241	−0.299	−0.304	−0.337	−0.328
XP ExposPenal	0.199	0.000	0.000	0.162	0.000	0.000	1.294	1.071	0.686
Glide posenum	3.000	95.000	7.000	2.000	7.000	7.000	1.000	1.000	1.000

(Sastry, et al., 2010; Chen, et al., 2023b). The data reveal intriguing insights into the properties and interactions of $DATT_n$ molecules. $DATT_9$ emerges with the highest number of any contacts, indicating extensive interactions with other

TABLE V
Interactions and Similarity Measures between $DATT_n$ Molecules and 8jzn-sit-4 Protein in *Candida albicans*

Title	$DATT_2$	$DATT_3$	$DATT_4$	$DATT_5$	$DATT_6$	$DATT_7$	$DATT_8$	$DATT_9$	$DATT_{10}$
SIFT any contact	16	19	20	22	21	23	26	27	21
SIFT backbone interaction	6	6	5	6	6	7	5	12	8
SIFT side chain interaction	15	18	20	20	21	21	26	23	18
SIFT polar residues	5	6	6	7	8	8	9	7	10
SIFT hydrophobic residues	10	12	14	13	13	13	17	16	8
SIFT hydrogen bond acceptor	0	0	0	0	0	0	0	0	0
SIFT hydrogen bond donor	0	0	0	0	0	0	0	0	1
SIFT aromatic residue	3	4	5	3	4	3	5	3	3
SIFT charged residue	2	2	2	2	2	2	3	2	3
Canvas means tanimoto similarity	0.513	0.58	0.548	0.553	0.518	0.464	0.425	0.467	0.4
Canvas max tanimoto similarity	1	1	1	1	1	1	1	1	1
Canvas max tanimoto similarity ID	129	128	127	126	123	125	122	124	130
Canvas min tanimoto similarity	0.265	0.337	0.286	0.355	0.312	0.273	0.254	0.349	0.254
Canvas min tanimoto similarity ID	130	130	130	130	130	122	130	129	122

TABLE VI
Docking Scores and Binding Characteristics for $DATT_n$ Molecules at Protein 8jzn-Site-4

Title	$DATT_2$	$DATT_3$	$DATT_4$	$DATT_5$	$DATT_6$	$DATT_7$	$DATT_8$	$DATT_9$	$DATT_{10}$
docking score	−8.122	−8.510	−9.248	−9.255	−9.760	−9.395	−9.760	−9.555	−2.279
XP GScore	−8.122	−8.510	−9.248	−9.255	−9.760	−9.395	−9.760	−9.555	−2.279
glide ligand efficiency	−0.254	−0.236	−0.231	−0.210	−0.203	−0.181	−0.174	−0.159	−0.036
glide emodel	−77.15	−89.46	−103.27	−103.81	−118.42	−112.64	−115.33	−112.43	−37.81
glide einternal	6.061	9.649	0.00	0.00	0.00	18.463	21.881	21.065	10.962
glide evdw	−52.87	−59.82	−62.33	−64.11	−67.38	−72.66	−76.96	−77.75	−65.03
XP Electro	−0.022	−0.051	0.012	−0.209	−0.200	−0.026	−0.070	−0.061	−0.105
XP HBond	0.00	0.00	0.00	0.00	−0.350	0.00	−0.160	0.00	−0.138
XP PhobEn	−0.850	−0.700	−0.840	−0.800	−0.556	−0.311	−0.625	−0.774	0.000
XP RotPenal	0.233	0.316	0.323	0.336	0.341	0.342	0.340	0.335	0.330
XP ExposPenal	0.000	0.143	0.00	0.00	0.314	0.00	0.065	0.859	1.860
Glide posenum	2	15	14	30	2	29	8	7	1

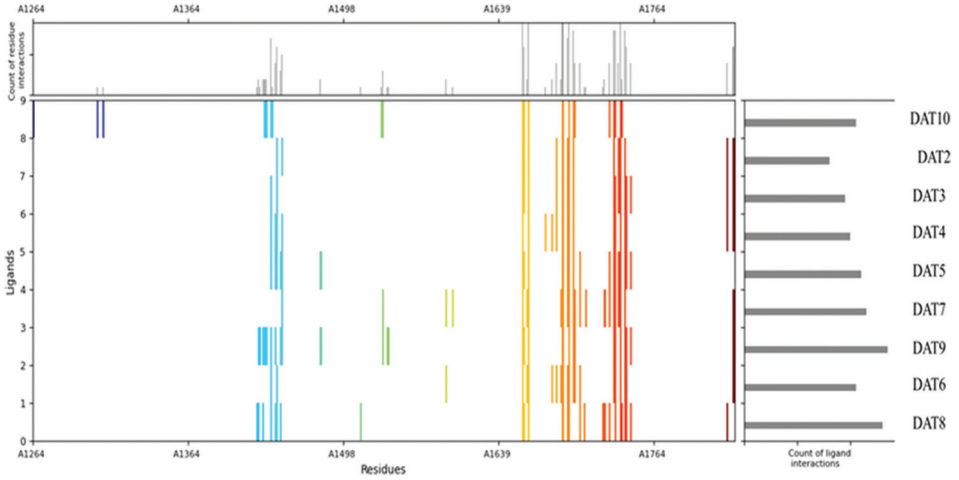

Fig. 2. Unveiling $DATT_n$ molecule interactions with 8JZN-sit-4 protein in *Candida albicans,* interaction fingerprint.

molecules. Meanwhile, $DATT_8$ leads in terms of side chain interactions and features a notable count of polar residues and hydrophobic residues, suggesting its versatility in molecular interactions. $DATT_{10}$ is distinctive for its hydrogen bond donor capabilities. Furthermore, the mean Tanimoto similarity score provides information on how structurally similar these molecules are to others in a chemical structure database, with $DATT_3$ displaying the highest similarity. In contrast, $DATT_7$ exhibits the lowest similarity. These values collectively shed light on the molecular characteristics and interactions of the $DATT_n$ molecules, which may be pertinent in various biological and chemical contexts (Rajitha, et al., 2021; Mamad, et al., 2024). $DATT_9$ has been selected for further investigation due to its promising attributes, including

low docking scores, favorable XP GlideScores, robust van der Waals interactions, and significant conformational flexibility with multiple binding poses. These characteristics suggest strong binding within the protein pocket.

F. Induced-Fit Docking (IFD): DATT9 with 8JZN

In Fig. 3, both the 3D and 2D interaction maps, derived from the Induced Fit docking of $DATT_9$ with the 8JZN-sit-4 protein in *C. albicans* using XP mode, clearly illustrate substantial alterations in the ligand's positioning and orientation within the binding site. These alterations reflect the adaptability of the protein pocket in response to induced fit docking. As a result of this flexibility, certain side chains or residues shift to optimize binding, leading to the accommodation of the ligand in various poses. Furthermore, the binding site volume, particularly in the interaction map between the protein and $DATT_9$, has also been modified due to the flexibility exhibited by both the protein and $DATT_9$. This adaptability in the binding site plays a crucial role in enabling different binding poses and interactions, ultimately influencing the ligand's binding behavior. In comparison between $DATT_9$ obtained through Glide-Dock_XP mode and $DATT_{91}$ to $DATT_{96}$ from InducedFit_XP mode, several crucial observations emerge in Table VII. First, the Prime Energy of $DATT_9$ is notably higher, indicating a less favorable energy state, whereas $DATT_{91}$ to $DATT_{96}$ exhibit highly

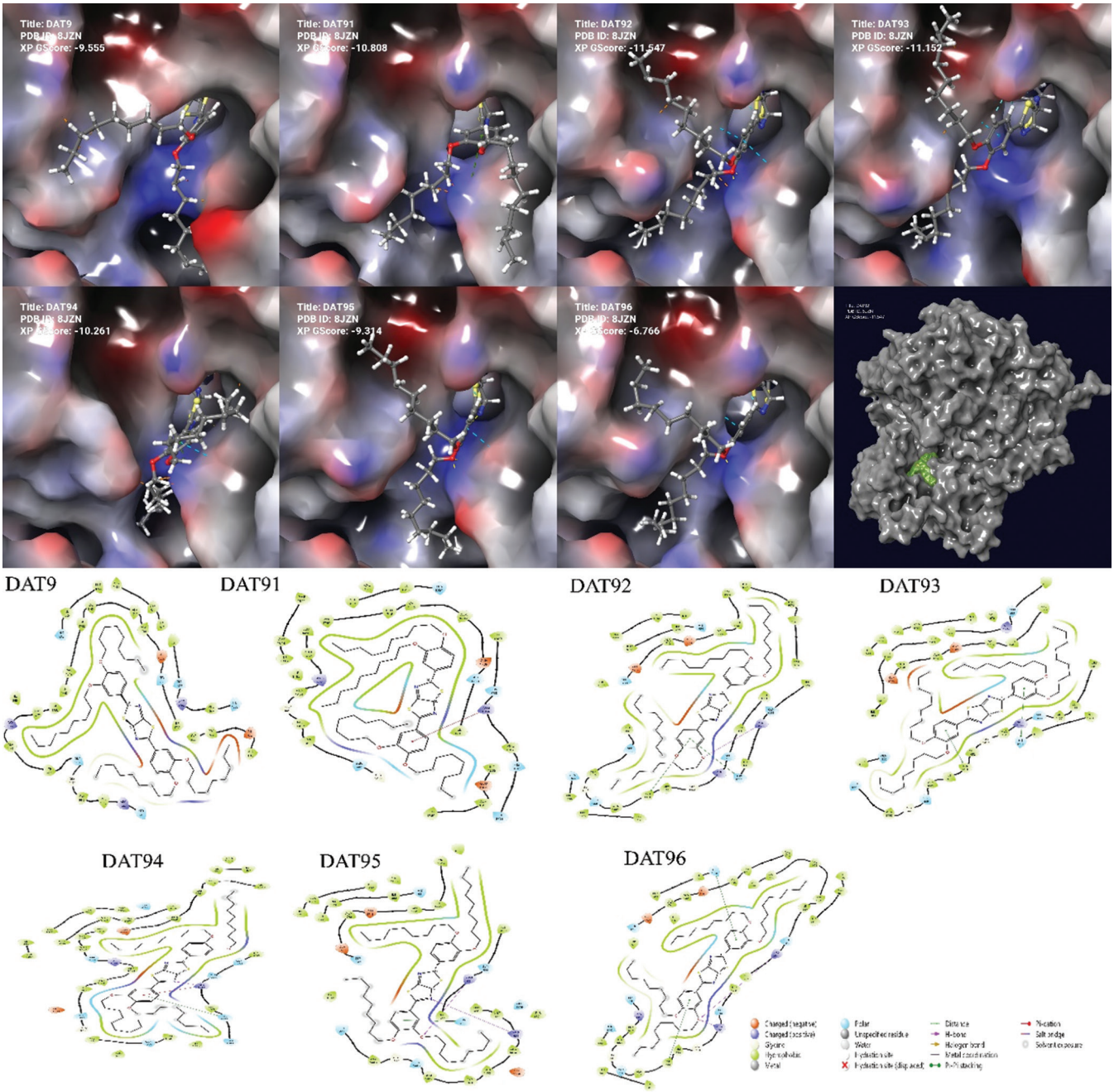

Fig. 3. 3D and 2D interaction maps of $DATT_9$ with 8JZN-sit-4 protein in *Candida albicans* using IFD-XP mode.

TABLE VII
Docking and Interaction Scores of $DATT_9$ with Multiple Poses Against 8jzn-sit-4 Protein in *Candida albicans* using (IFD-XP Mode)

Title	$DATT_9$	$DATT_{91}$	$DATT_{92}$	$DATT_{93}$	$DATT_{94}$	$DATT_{95}$	$DATT_{96}$
Glide ligand efficiency	−0.159	−0.180	−0.192	−0.186	−0.171	−0.155	−0.113
Docking score	−9.555	−10.808	−11.547	−11.152	−10.261	−9.314	−6.766
XP GScore	−9.555	−10.808	−11.547	−11.152	−10.261	−9.314	−6.766
Glide evdw	−77.755	−87.116	−90.445	−89.558	−82.374	−82.197	−88.358
Glide ecoul	−0.807	−0.660	−4.439	−2.381	0.170	−3.713	−2.342
Glide energy	−78.562	−87.776	−94.884	−91.939	−82.204	−85.910	−90.701
Glide einternal	21.065	17.232	14.207	20.107	24.761	17.440	21.516
Glide emodel	−112.434	−131.887	−168.887	−153.724	−123.005	−148.729	−150.178
XP HBond	0.000	0.000	−0.660	0.000	0.000	−0.505	−0.428
XP PhobEn	−0.774	−0.799	−1.150	−0.950	−1.071	−1.075	−1.004
XP PhobEnHB	0.000	0.000	0.000	0.000	0.000	0.000	0.000
XP LowMW	0.000	0.000	0.000	0.000	0.000	0.000	0.000
XP RotPenal	0.335	0.335	0.335	0.335	0.335	0.335	0.335
XP LipophilicEvdW	−9.480	−11.450	−9.947	−10.194	−9.701	−9.198	−10.012
XP Electro	−0.061	−0.050	−0.333	−0.179	0.013	−0.278	−0.176
XP ExposPenal	0.859	0.721	0.781	0.106	0.405	0.714	1.030
Glide posenum	7.000	6.000	2.000	7.000	1.000	1.000	1.000
Prime energy	3,224.8	−62,714.7	−62,698.9	−62,701.0	−62,706.4	−62,714.0	−62,714.7
Interaction map area	1627.451	1593.710	1594.665	1656.250	1560.356	1688.436	1528.935
IFD score		−3,146.540	−3,146.490	−3,146.200	−3,145.580	−3,145.010	−3,142.500

negative values, signifying a substantial reduction in energy during induced fit docking. This highlights the improved energetically favorable interactions between the ligand and protein in the induced fit poses. Glide Ligand Efficiency, although slightly lower in $DATT_{91}$ to $DATT_{96}$, is a common trend in induced fit docking, where ligands adapt to precise protein pockets at the expense of higher energy penalties. Second, in terms of the Docking Score (XP GScore), $DATT_9$ presents a score of approximately −9.56, whereas $DATT_{91}$ to $DATT_{96}$ consistently exhibit lower, more negative scores. These lower scores represent enhanced binding affinity and energy minimization in the induced fit poses, showcasing the optimization of ligand-protein interactions. Moreover, the Van der Waals energy (Glide evdw) is reduced in $DATT_{91}$ to $DATT_{96}$, implying improved Van der Waals interactions as ligands better fit protein binding sites, reducing steric clashes. In addition, the electrostatic energy (Glide ecoul) shows less negative values in $DATT_9$ compared to $DATT_{91}$ to $DATT_{96}$, implying optimized electrostatic interactions in induced fit docking. Lower internal energy (Glide einternal) in $DATT_{91}$ to $DATT_{96}$ reflects improvements achieved in internal energy contributions through induced fit docking, which may be linked to favorable ligand conformations in binding sites. The variations in XP HBond values from $DATT_{91}$ to $DATT_{96}$ indicate changes in hydrogen bond formation or disruption during induced fit docking, which can significantly impact binding specificity and strength. Furthermore, the XP Lipophilic EvdW values in $DATT_{91}$ to $DATT_{96}$ are generally lower, demonstrating enhanced hydrophobic interactions typical of induced fit docking. Finally, XP ExposPenal values differ, reflecting changes in exposure energy penalties due to ligand or protein conformational alterations during induced fit docking. The varying number of generated poses among $DATT_{91}$ to $DATT_{96}$ underscores the conformational adaptability of ligands and proteins during the induced fit docking process. This comprehensive comparison reveals the benefits of induced fit docking, resulting in improved binding affinity, energy minimization, and more optimized ligand-protein interactions. These parameter changes signify the ligand's capacity to conform more favorably to the specific binding site, ultimately achieving more energetically favorable poses.

G. Exploring Ligand-Protein Interactions (S. aureus and E. coli)

After conducting molecular docking simulations using Glide-Dock in XP mode, an advanced and highly accurate docking mode within the Schrödinger suite, with $DATT_n$ molecules in various binding pockets of the 5M18 and 3N8D proteins from *S. aureus* bacteria and the 6RKU protein in *E. coli*, we delved deep into the intricate molecular interactions at play (Fig. 4). Glide's XP mode acted, such as a magnifying glass, allowing us to scrutinize the ligand-protein binding with exceptional precision. This in-depth analysis provided us with valuable insights into the binding affinities and potential of these $DATT_n$ molecules as drug candidates. The data from all pockets were carefully analyzed. Subsequently, the most promising sites were identified and are referred to as "5M18_site_1," "3N8D-site_2," and "6RKU_site_2" in Table III. However, it is important to note that the data obtained from docking $DATT_n$ molecules into these specific pockets (Table IV) do not indicate a strong interaction between the molecules and both proteins in *S. aureus* and the 6RKU protein of *E. coli*. This suggests that these molecules may not effectively bind to the proteins. This observation aligns with the *in vitro* results presented in Table II, which also suggest that the compounds are not effective in inhibiting the growth of *S. aureus* and *E. coli* microbes.

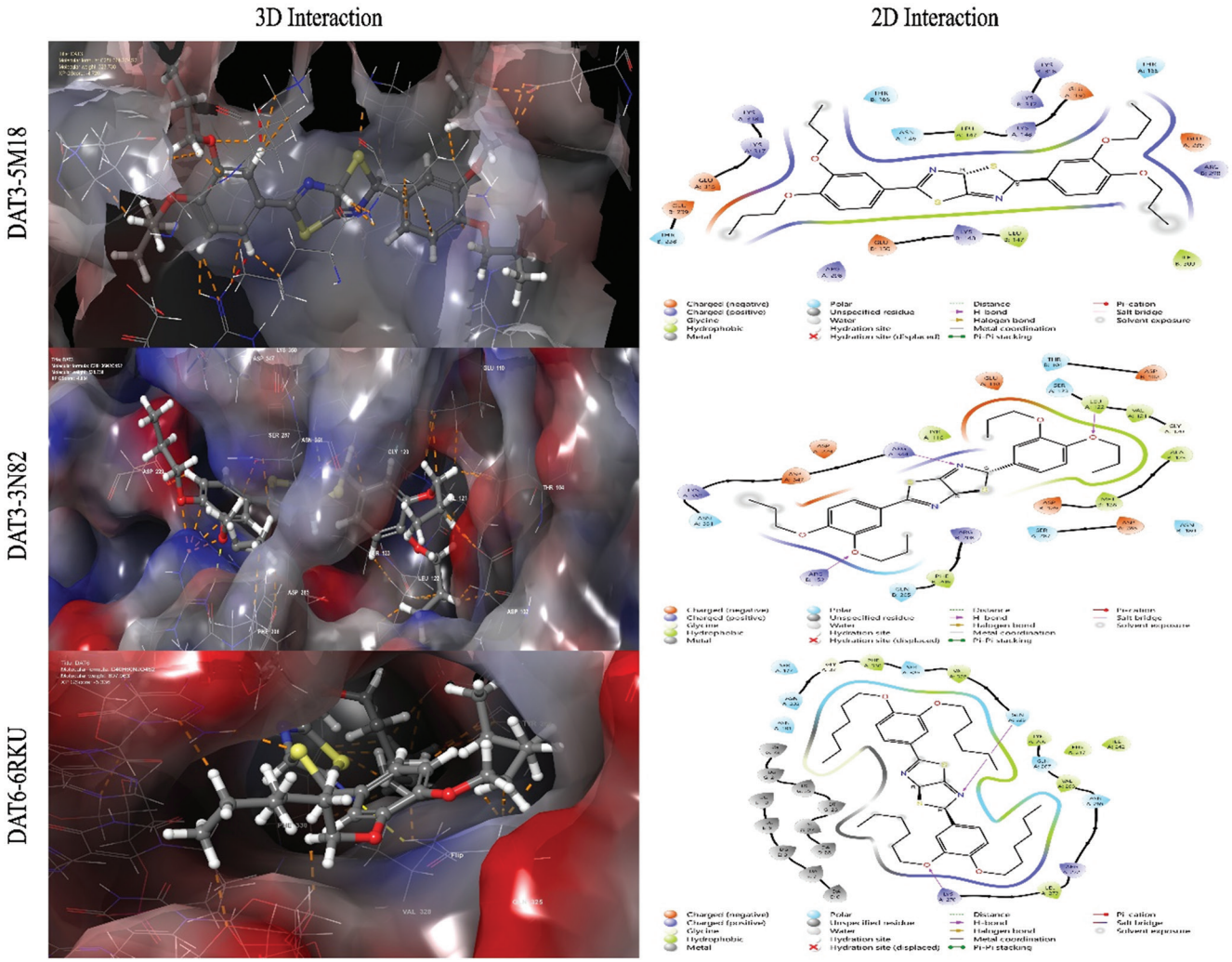

Fig. 4. Protein-ligand interaction maps and electrostatic surfaces for docked $DATT_3$ on *Staphylococcus aureus* proteins (Portion Data Bank [PDB]: 3N82 and 5M18) and $DATT_6$ on *Escherichia coli* protein (PDB: 6RKU) in 2D and 3D.

H. Molecular Descriptors $DATT_2$-$DATT_{10}$

In Maestro Schrodinger software, molecular descriptors tool has been used for the prediction of topological descriptors, QikProp properties, semiempirical properties (method to use for SE calculation PM7) through geometry optimization and QikProp 4.4 user manual was employed to evaluate the descriptor values and determine recommended ranges for each descriptor (Hostaš, Řezáč, and Hobza, 2013), and several of these parameters have been shown in Table VIII. The analysis of $DATT_n$ molecules in Table VIII offers crucial insights into their pharmaceutical characteristics. Notably, the molecular weights (ranging from 472.616 to 921.474 amu) deviate for some $DATT_n$ molecules from the typical drug range, potentially influencing their suitability in drug development, particularly with regard to factors, such as drug absorption and distribution. In addition, the i_qp_#stars values indicate that $DATT_4$ to $DATT_{10}$ possess unique properties compared to established drugs. The i_qp_#rotor values, ranging from 8 to 40, indicate an increased structural flexibility in these molecules, potentially impacting their applicability. A uniform i_qp_#rtvFG value of 0 reduces the risk of false positives in screening assays. In terms of central nervous system (CNS) activity (i_qp_CNS), most $DATT_n$ molecules are inactive. Dipole moments, predominantly within the expected range of 1.0–12.5, suggest balanced charge distribution, while the absence of hydrogen bonding points to limited interaction with water. The analysis of the First Zagreb index (i_desc_First_Zagreb) highlights size variations among these molecules, with $DATT_{10}$ being the largest and $DATT_2$ the smallest. Solvent-accessible surface area (SASA) values for $DATT_5$ to $DATT_{10}$ indicate larger-than-typical values, possibly impacting molecular interactions and biological activity. Furthermore, $DATT_n$ molecules align with the recommended hydrophobic properties (r_qp_FOSA) for drugs. The π component of the SASA (r_qp_PISA) offers insights into surface area properties related to carbon and attached hydrogen atoms. Polar surface area (PSA) values fall within the expected range, indicating relatively small PSAs. Hydrophilic components remain within the recommended range. Finally, weakly PSA properties (r_qp_WPSA) exhibit variations among $DATT_n$ molecules, presenting a comprehensive overview of their unique pharmaceutical

TABLE VIII
Deciphering DATTn Molecules: Topological, Qikprop, and Semiempirical Revelations

No.	Property or descriptor	DAT_T2	$DATT_3$	$DATT_4$	$DATT_5$	$DATT_6$	$DATT_7$	$DATT_8$	$DATT_9$	$DATT_{10}$	Range or recommended values
1.	r_qp_mol_MW	472.62	528.72	584.83	640.94	697.05	753.15	809.26	865.37	921.47	130.0–725.0
2.	i_qp_#stars	1.00	3.00	6.00	9.00	10.00	11.00	11.00	12.00	12.00	0–5
3.	i_qp_#rotor	8.00	12.00	16.00	20.00	24.00	28.00	32.00	36.00	40.00	0–15
4.	i_qp_#rtvFG	0.00	0.00	0.00	0.00	0.00	0.00	0.00	0.00	0.00	0–2
5.	i_qp_CNS	0.00	0.00	0.00	−1.00	−2.00	−2.00	−2.00	−2.00	−2.00	–2.0–2
6.	r_mopac_Dipole	1.57	3.73	1.84	3.96	3.83	3.14	4.63	1.73	1.50	1–−12
7.	r_qp_volume	1,489.67	1,677.13	1,886.26	2,051.56	2,380.64	2,616.12	2,836.69	3,074.95	3,339.37	500–2000
8.	i_desc_First_Zagreb	166.00	182.00	198.00	214.00	230.00	246.00	262.00	278.00	294.00	
9.	r_qp_SASA	836.48	915.65	995.33	1,064.24	1,279.87	1,389.27	1,519.60	1,633.93	1,787.42	300–1000
10.	r_qp_FOSA	527.46	620.98	733.70	802.52	1,012.32	1,124.63	1,230.41	1,370.91	1,515.75	0–750
11.	r_qp_PISA	198.61	183.21	157.90	158.37	177.55	146.32	168.02	175.75	162.88	0–450
12.	r_qp_PSA	43.94	43.67	47.57	46.42	42.48	47.89	45.43	47.79	43.69	7.0–200
13.	r_qp_FISA	31.54	29.18	32.03	26.51	21.28	33.64	34.72	19.67	31.46	7–330
14.	r_qp_WPSA	78.87	82.28	71.70	76.84	68.72	84.68	86.45	67.61	77.33	0.0–175.0
15.	r_qp_donorHB	0.00	0.00	0.00	0.00	0.00	0.00	0.00	0.00	0.00	0–6
16.	r_qp_accptHB	6.50	6.50	6.50	6.50	6.50	6.50	6.50	6.50	6.50	0.0–20.0
17.	r_qp_QPpolrz	50.22	55.01	60.57	64.62	75.41	81.96	88.43	95.47	103.36	13–70
18.	r_qp_QPlogPo/w	6.16	7.40	8.67	9.81	11.98	13.46	14.92	16.52	18.18	–2.0–6.5
19.	r_qp_QPlogS	−7.71	−8.57	−9.38	−10.06	−13.46	−14.95	−16.78	−18.21	−20.51	–6.5–0.5
20.	r_qp_QPlogKp	−0.63	−0.26	−0.02	0.47	1.02	1.06	1.51	2.19	2.32	–8.0–−1.0
21.	r_qp_QPPMDCK	7,577.53	8,365.19	6,843.61	8,317.08	8,494.52	7,761.02	7,734.32	8,701.66	7,445.97	<25 poor, >500 great
22.	r_qp_QPPCaco	4,975.04	5,238.45	4,922.62	5,552.44	6,224.53	4,752.50	4,641.00	6,447.90	4,983.75	<25 poor, >500 great
23.	r_qp_QPlogBB	−0.10	−0.31	−0.61	−0.78	−1.03	−1.43	−1.72	−1.78	−2.23	–3.0–1.2
24.	r_qp_PercentHumanOralAbsorption	100.00	100.00	100.00	100.00	100.00	100.00	100.00	100.00	100.00	>80% is high
25.	i_qp_RuleOfFive	1.00	2.00	2.00	2.00	2.00	2.00	2.00	2.00	2.00	Maximum is 4
26.	i_qp_RuleOfThree	2.00	2.00	2.00	2.00	2.00	2.00	2.00	2.00	2.00	Maximum is 3
27.	r_mopac_HOMO_Energy	−8.42	−8.41	−8.56	−8.43	−8.40	−8.72	−8.48	−8.56	−8.50	PM7
28.	r_mopac_LUMO_Energy	−0.96	−0.85	−0.92	−0.88	−0.89	−0.91	−0.86	−0.83	−0.95	PM7
29.	r_mopac_MOPAC_Total_Energy_EV	−5,231.4	−5,831.2	−6,431.0	−7,030.8	−7,630.6	−8,230.5	−8,830.3	−9,421.0	−10,030.1	PM7
30.	r_mopac_MOPAC_Heat_of_Formation	−70.23	−91.10	−113.18	−134.85	−150.92	−174.29	−192.48	−206.67	−234.73	PM7

SASA: Solvent-accessible surface area, WPSA: Weakly polar surface area, CNS: Central nervous system, HOMO: Highest occupied molecular orbital, LUMO: Lowest unoccupied molecular orbital

attributes. In the examination of the $DATT_n$ molecules ($DATT_2$ to $DATT_{10}$), a spectrum of significant characteristics and descriptors emerges. Evidently, these molecules manifest limited propensity for hydrogen bonding with water, denoted by an estimated average of zero hydrogen bonds donated to water molecules, juxtaposed with their capacity to accept an average of 6.5 hydrogen bonds from water. Their polarizability values indicate variations in their interaction potential, with $DATT_6$ to $DATT_{10}$ exceeding the conventional range. Moreover, the r_qp_QPlogPo/w descriptor highlights deviations in their affinity for organic solvents over water, which may impact solubility and distribution. Their aqueous solubility levels suggest potential obstacles, with all $DATT_n$ molecules encountering difficulties in achieving aqueous solubility. Strikingly, these compounds exhibit elevated skin permeability and the ability to effectively transgress the blood–brain barrier, promising prospects for dermal drug delivery and CNS interaction. Their adherence to Lipinski's rule of five underscores their drug-like attributes, although Jorgensen's rule of three implies potential challenges in oral availability. The analysis of electronic structure unveils fluctuations in highest occupied molecular orbital and lowest unoccupied molecular orbital energy levels, signifying shifts in reactivity and stability (Omer, et al., 2020; Ahmed and Omer, 2021). A progressive trend of stability, as indicated by diminishing MOPAC total energy and heat of formation values, positions $DATT_n$ molecules for multifaceted applications in the pharmaceutical and chemical domains.

IV. Conclusion

The synthesis and assessment of $DATT_n$ compounds have unveiled their potential as promising antimicrobial agents. Our *in vitro* experiments have unveiled their remarkable antifungal activity against *C. albicans*, offering a promising avenue for combatting fungal infections. Nevertheless, it is crucial to acknowledge the limited efficacy of these compounds against *S. aureus* and *E. coli*, two clinically significant bacterial strains. The *in silico* molecular docking studies, conducted using the Schrödinger suite, have yielded valuable insights into the interactions between $DATT_n$ compounds and specific target proteins within these pathogens. Particularly, the robust binding affinity observed between $DATT_n$ compounds and the 8JZN protein in *C. albicans* suggests their suitability as potential drug candidates for treating fungal infections. The combined results from our *in vitro* and *in silico* investigations underscore the multifaceted nature of $DATT_n$ compounds,

emphasizing their promise as antifungal agents. Subsequent research and clinical trials are imperative to fully explore their therapeutic potential, evaluate their safety profile, and establish their efficacy for clinical applications.

Acknowledgment

Authors would like to express our gratitude to Koya University's Chemistry Department for their assistance and support in our endeavor.

References

Abad-Zapatero, C., and Metz, J.T., 2005. Ligand efficiency indices as guideposts for drug discovery. *Drug Discovery Today*, 10, pp.464-469.

Ahmed, L., and Omer, R., 2021. 1H-pyrrole, furan, and thiophene molecule corrosion inhibitor behaviors. *Journal of Physical Chemistry and Functional Materials*, 4, pp.1-4.

Al-Mutabagani, L.A., Alshabanah, L.A., Gomha, S.M., Abolibda, T.Z., Shaban, M., and Ahmed, H.A., (2021). Synthesis and mesomorphic and electrical investigations of new furan liquid crystal derivatives. *Frontiers in Chemistry*, 9, p.711862.

Anwar Omar, R., Koparir, P., Koparir, M., and Safin, D.A., 2023. A novel cyclobutane-derived thiazole-thiourea hybrid with a potency against COVID-19 and tick-borne encephalitis: Synthesis, characterization, and computational analysis. *Journal of Sulfur Chemistry*, 45, pp.1-18.

Atmaram, U.A., and Roopan, S.M., 2022. Biological activity of oxadiazole and thiadiazole derivatives. *Applied Microbiology and Biotechnology*, 106, pp.3489-3505.

Beinat, C., 2014. *The Design and Synthesis of Selective α7 Nicotinic Acetylcholine Receptor Agonists for the Treatment of Neurological Disease*. The University of Sydney, Sydney.

Chen, W., Cui, D., Jerome, S.V., Michino, M., Lenselink, E.B., Huggins, D.J., Beautrait, A., Vendome, J., Abel, R., Friesner, R.A., and Wang, L., 2023a. Enhancing hit discovery in virtual screening through absolute protein-ligand binding free-energy calculations. *Journal of Chemical Information and Modeling*, 63, pp.3171-3185.

Chen, W., Cui, D., Jerome, S.V., Michino, M., Lenselink, E.B., Huggins, D.J., Beautrait, A., Vendome, J., Abel, R., Friesner, R.A., and Wang, L., 2023b. Enhancing hit discovery in virtual screening through absolute protein-ligand binding free-energy calculations. *Journal of Chemical Information and Modeling*, 63, pp.3171-3185.

Erdoğan, M., Taslimi, P., and Tuzun, B., 2021. Synthesis and docking calculations of tetrafluoronaphthalene derivatives and their inhibition profiles against some metabolic enzymes. *Archiv der Pharmazie*, 354, p.2000409.

Farid, R., Day, T., Friesner, R.A., and Pearlstein, R.A., 2006. New insights about HERG blockade obtained from protein modeling, potential energy mapping, and docking studies. *Bioorganic and Medicinal Chemistry*, 14, pp.3160-3173.

Fishovitz, J., Hermoso, J.A., Chang, M., and Mobashery, S., 2014. Penicillin-binding protein 2a of methicillin-resistant *Staphylococcus aureus*. *IUBMB Life*, 66, pp.572-577.

Gulcin, İ., Petrova, O.V., Taslimi, P., Malysheva, S.F., Schmidt, E.Y., Sobenina, L.N., Gusarova, N.K., Trofimov, B.A., Tuzun, B., and Farzaliyev, V.M., 2022. Synthesis, characterization, molecular docking, acetylcholinesterase and α-glycosidase inhibition profiles of nitrogen-based novel heterocyclic compounds. *ChemistrySelect*, 7, p.e202200370.

Halgren, T.A., 2009. Identifying and characterizing binding sites and assessing druggability. *Journal of Chemical Information and Modeling*, 49, pp.377-389.

Hamad, W.M., Aziz, H.J., and Al-Dujaili, A.H., 2004. Synthesis and liquid crystalline studies of some heterocyclic compounds with lateral long chain substituents. *ZANCO Journal of Pure and Applied Sciences*, 16, pp.63-69.

Hopkins, A.L., Keserü, G.M., Leeson, P.D., Rees, D.C., and Reynolds, C.H., 2014. The role of ligand efficiency metrics in drug discovery. *Nature Reviews Drug Discovery*, 13, pp.105-121.

Hostaš, J., Řezáč, J., and Hobza, P., 2013. On the performance of the semiempirical quantum mechanical PM6 and PM7 methods for noncovalent interactions. *Chemical Physics Letters*, 568, pp.161-166.

Jakhar, R., Khichi, A., Kumar, D., Sura, K., Bhoomika, Dangi, M., and Chhillar, A.K., 2022. Development of pharmacophore model to identify potential DNA gyrase inhibitors. *Journal of Biomolecular Structure and Dynamics*, 41, pp.10125-10135.

Jays, J., Mohan, S., and Saravanan, J., 2019. Molecular docking studies of novel aminopyrimidines as potent antifungal agents. *Chemical Methodologies*, 3, pp.442-450.

Kaka, K.N., Omer, R.A., Mamand, D.M., and Qader, A.F., 2024. Bromination of chalcone: Study on synthesis, characterization, and optoelectronic properties. *Aro-The Scientific Journal of Koya University*, 12, pp.48-53.

Khan, F., Jeong, G.J., Javaid, A., Thuy Nguyen Pham, D., Tabassum, N., and Kim, Y.M., 2023. Surface adherence and vacuolar internalization of bacterial pathogens to the *Candida* spp. cells: Mechanism of persistence and propagation. *Journal of Advanced Research*, 53, pp.115-136.

Koparir, P., Anwar Omar, R., Sarac, K., Koparir, M., and Safin, D.A., 2023a. Novel 1, 2, 4-triazolethiol-thiophen Hybrids: Facile synthesis, characterization, ADMET prediction and molecular docking. *Polycyclic Aromatic Compounds*, 6, pp.1-15

Koparir, P., Omar, R.A., Sarac, K., Ahmed, L.O., Karatepe, A., Taskin-Tok, T., and Safin, D.A., 2023b. Synthesis, characterization and computational analysis of thiophene-2, 5-diylbis ((3-mesityl-3-methylcyclobutyl) methanone). *Polycyclic Aromatic Compounds*, 43, pp.6107-6125.

Koparir, P., Parlak, A.E., Karatepe, A., and Omar, R.A., 2022. Elucidation of potential anticancer, antioxidant and antimicrobial properties of some new triazole compounds bearing pyridine-4-yl moiety and cyclobutane ring. *Arabian Journal of Chemistry*, 15, p.103957.

Lebreton, F., and Cattoir, V., 2019. Resistance to glycopeptide antibiotics. In: *Bacterial Resistance to Antibiotics: From Molecules to Man*. John Wiley and Sons, United States, pp.51-80.

Liu, J., and Balasubramanian, M.K., 2001. 1,3-beta-Glucan synthase: A useful target for antifungal drugs. *Current Drug Targets-Infectious Disorders*, 1, pp.159-169.

Mahasenan, K.V., Molina, R., Bouley, R., Batuecas, M.T., Fisher, J.F., Hermoso, J.A., Chang, M., and Mobashery, S., 2017. Conformational dynamics in penicillin-binding protein 2a of methicillin-resistant *Staphylococcus aureus*, allosteric communication network and enablement of catalysis. *Journal of the American Chemical Society*, 139, pp.2102-2110.

Mamad, D.M., Azeez, Y.H., Kaka, A.K., Ahmed, K.M., Omer, R.A., and Ahmed, L.O., 2024. The inhibitor activity of some azo compound derivatives using density functional theory and molecular dynamics simulations. *Computational and Theoretical Chemistry*, 1237, p.114645.

Moravej, H., Moravej, Z., Yazdanparast, M., Heiat, M., Mirhosseini, A., Moosazadeh Moghaddam, M., and Mirnejad, R., 2018. Antimicrobial peptides: Features, action, and their resistance mechanisms in bacteria. *Microbial Drug Resistance*, 24, pp.747-767.

Naghiyev, F., Mamedov, I., Askerov, R., Taslimi, P., and Poustforoosh, A., 2022. Synthesis and biological activity of functionally substituted pyrimidine and pyran derivatives on the basis of isatylidene malononitriles. *ChemistrySelect,* 7, p.e202202006.

Nöllmann, M., Crisona, N.J., and Arimondo, P.B., 2007. Thirty years of

Escherichia coli DNA gyrase: From *in vivo* function to single-molecule mechanism. *Biochimie*, 89, pp.490-499.

Omar, R.A., Koparir, P., Sarac, K., Koparir, M., and Safin, D.A., 2023a. A novel coumarin-triazole-thiophene hybrid: Synthesis, characterization, ADMET prediction, molecular docking and molecular dynamics studies with a series of SARS-CoV-2 proteins. *Journal of Chemical Sciences* (*Bangalore*), 135, p.6.

Omar, R.A., Omar, K.A., and Abdullah, B.A., 2016a. Polyaniline: Synthesis, characterizations and study their antibacterial activity against *Escherichia coli*. *Journal of Chemical, Biological and Physical Sciences,* 6, p.510.

Omar, R.A., Smail, A.K., and Omar, K.A., 2016b. Study on the activity of Ag/Nylon 6, 10 nanocomposite against *Escherichia coli*. *International Journal of Current Microbiology and Applied Sciences*, 5, pp.935-941.

Omar, S.Y., Mamand, D.M., Omer, R.A., Rashid, R.F., and Salih, M.I., 2023b. Investigating the role of metoclopramide and hyoscine-N-Butyl bromide in colon motility. *ARO-The Scientific Journal of Koya University*, 11, pp.109-115.

Omer, R.A., Ahmed, L.O., Koparir, M., and Koparir, P., 2020. Theoretical analysis of the reactivity of chloroquine and hydroxychloroquine. *Indian Journal of Chemistry*, 59A, pp.1828-1834.

Omer, R.A., Gheni, A.I., Omar, K.A., and Ahmed, L.O., 2019. Antimicrobial activity of nylon nanocomposites against *Staphylococcus aureus* and *Escherichia coli* bacteria. *Science Journal of University of Zakho*, 7, pp.138-143.

Omer, R.A., Koparir, P., and Koparir, M., 2023a. Synthesis, experimental characterization, DFT and theoretical anticorrosion study for 1-(4-(3-Methyl-3-phenylcyclobutyl) thiazol-2-yl)-3-(p-tolyl) thiourea. *Protection of Metals and Physical Chemistry of Surfaces*, 59, pp.1315-1325.

Omer, R.A., Mustafa, R.A., Salih, S., Hamad, W., and Taher, S., 2023b. Synthesis of a new series of benzothiazole compounds and study of their liquid crystal properties. *Passer Journal of Basic and Applied Sciences*, 5, pp.78-84.

Paymal, S.B., Barale, S.S., Supanekar, S.V., and Sonawane, K.D., 2023. Structure based virtual screening, molecular dynamic simulation to identify the oxadiazole derivatives as inhibitors of *Enterococcus* D-Ala-D-Ser ligase for combating vancomycin resistance. *Computers in Biology and Medicine*, 159, p.106965.

Rajitha, G., Rani, M.V., Vankadoth, U.N., and Umamaheswari, A., 2021. Design of novel selective estrogen receptor inhibitors using molecular docking and protein-ligand interaction fingerprint studies. *Journal of Pharmaceutical Research International*, 33, pp.470-483.

Rementeria, A., López-Molina, N., Ludwig, A., Vivanco, A.B., Bikandi, J., Pontón, J., and Garaizar, J., 2005. Genes and molecules involved in *Aspergillus fumigatus* virulence. *Revista Iberoamericana de Micología*, 22, pp.1-23.

Ruer, S., Pinotsis, N., Steadman, D., Waksman, G., and Remaut, H., 2015. Virulence-targeted antibacterials: Concept, promise, and susceptibility to resistance mechanisms. *Chemical Biology and Drug Design*, 86, pp.379-399.

Salih, S.K., Mustafa, R.M., Mamad, D.M., Kaka, K.N., Omer, R.A., and Hamad, W.M., 2023. Synthesis of liquid crystalline benzothiazole based derivatives: Theoretical and experimental study of their optical and electrical properties. *ZANCO Journal of Pure and Applied Sciences*, 35, pp.143-162.

Sandor, M., Kiss, R., and Keserű, G.R.M., 2010. Virtual fragment docking by Glide: A validation study on 190 protein-fragment complexes. *Journal of Chemical Information and Modeling*, 50, pp.1165-1172.

Sarafroz, M., Siddiqui, S.A., and Yar, M.S., 2020. Synthesis, antimicrobial, and molecular docking studies of 1, 3-thiazolidin-4-one analogs bearing benzothiazole. *Indian Journal of Heterocyclic Chemistry*, 30, pp.325-335

Sastry, M., Lowrie, J.F., Dixon, S.L., and Sherman, W., 2010. Large-scale systematic analysis of 2D fingerprint methods and parameters to improve virtual screening enrichments. *Journal of Chemical Information and Modeling*, 50, pp.771-784.

Tripathi, S.K., Selvaraj, C., Singh, S.K., and Reddy, K.K., 2012. Molecular docking, QPLD, and ADME prediction studies on HIV-1 integrase leads. *Medicinal Chemistry Research*, 21, pp.4239-4251.

Vass, M., Tarcsay, Á., and Keserű, G.M., 2012. Multiple ligand docking by Glide: Implications for virtual second-site screening. *Journal of Computer-Aided Molecular Design*, 26, pp.821-834.

Verma, A.K., Ahmed, S.F., Hossain, M.S., Bhojiya, A.A., Mathur, A., Upadhyay, S.K., Srivastava, A.K., Vishvakarma, N.K., Barik, M., and Rahaman, M.M., 2022. Molecular docking and simulation studies of flavonoid compounds against PBP-2a of methicillin-resistant *Staphylococcus aureus*. *Journal of Biomolecular Structure and Dynamics,* 40, pp.10561-10577.

Zhao, C.R., You, Z.L., Chen, D.D., Hang, J., Wang, Z.B., Ji, M., Wang, L.X., Zhao, P., Qiao, J., and Yun, C.H., 2023. Structure of a fungal 1, 3-β-glucan synthase. *Science Advances*, 9, p.eadh7820.